Nuclear Instruments and Methods in Physics Research B 267 (2009) 330–333

Contents lists available at ScienceDirect

Nuclear Instruments and Methods in Physics Research B

journal homepage: www.elsevier.com/locate/nimb

Carrier-envelope phase dependence in atomic ionization by short-laser pulses

D.G. Arbó [a,b,*], E. Persson [b], K.I. Dimitriou [c,d], J. Burgdörfer [b]

[a] Institute for Astronomy and Space Physics, IAFE, CC 67, Suc. 28 (1428) Buenos Aires, Argentina
[b] Institute for Theoretical Physics, Vienna University of Technology, Vienna, Austria
[c] Physics Department, National Technical University, Athens, Greece
[d] Theoretical and Physical Chemistry Institute, National Hellenic Research Foundation, Athens, Greece

ARTICLE INFO

Available online 22 October 2008

PACS:
32.80.Rm
32.80.Fb
03.65.Sq

Keywords:
Carrier-envelope phase
Short-laser pulse
Angular momentum

ABSTRACT

In atomic ionization by few-cycle laser pulses doubly differential momentum distributions near-threshold exhibit a radial nodal structure that results from peaked partial-wave distributions near a particular angular momentum. We analyze the doubly differential momentum distribution for different carrier-envelope phases. We find that in the cases where the photoelectron reaches a minimum at threshold the angular momentum distribution is very sensitive to the CEP since small variations of the ponderomotive energy can lead to the opening or closing of a new channel.

1. Introduction

The interaction of few-cycle pulses with matter has attracted considerable interest as shorter laser pulses have become available. Ultrashort pulses for which the pulse length τ becomes comparable to the optical period T lead to novel features of laser–matter interactions, among them are the strong carrier-envelope phase (CEP) dependence of excitation and ionization processes [1–3]. Rudenko et al. [4] and Maharjan et al. [5] presented fully two-dimensional momentum maps for laser-ionized electrons for different rare gases. The near-threshold structures observed have recently been semiclassically explained in terms of a classical angular momentum distribution sharply peaked [6,7] near the quantum number l_0. Such distributions in the near-threshold continuum result from the interplay between the laser and the Coulomb fields [8,9]. The existence of subpeaks in the photoelectron spectra of rare-gas atoms was explained by the rapidly changing ponderomotive potential in the short laser pulse [10]. The effect of channel closing on the photoionization yield has been extensively studied [11–13].

In the present work we study the CEP-dependence of the momentum distributions of ejected electrons. We show that the dominant angular momentum distribution near-threshold is sensitive to variations in the CEP in the case that a new channel appears, that is, when there is a minimum of the photoelectron spectrum very close to threshold. Here, the CEP-dependence of the ponderomotive energy leads to a CEP-dependence of the doubly differential momentum distributions. Atomic units are used throughout.

2. Carrier-envelope phase dependent ponderomotive energy

We consider an atom interacting with a linearly polarized laser field. Within the single active electron approximation the Hamiltonian is

$$H = \frac{\vec{p}^2}{2} + V(r) + \vec{r}\cdot\vec{F}(t), \tag{1}$$

where $\vec{p}$ and $\vec{r}$ are the momentum and position of the electron, respectively, $V(r)$ is the atomic central potential, and $\vec{F}(t)$ is the time dependent external field, which we choose as

$$\vec{F}(t) = F_0 \cos^2\left(\frac{\pi t}{\tau}\right)\cos(\omega t + \varphi_{CE})\hat{z}; \quad -\tau/2 \leqslant t \leqslant \tau/2, \tag{2}$$

and zero elsewhere. In Eq. (2), ω is the laser carrier frequency, φ_{CE} is the carrier-envelope phase, τ is the total pulse duration, F_0 is the peak field and $\hat{z}$ is the polarization direction.

The maximum field $F_{\max}$ reached according to Eq. (2) depends on the CEP for short pulses. For a cosine pulse, i.e. $\varphi_{CE} = 0$, the value of $F_{\max}$ coincides with the peak field F_0 while for any other value of the CEP $F_{\max} < F_0$. We define a CEP-dependent ponderomotive energy related to the field maximum of the pulse as

$$U_p(\varphi_{CE}) = \frac{[F_{\max}(\varphi_{CE})]^2}{4\omega^2}. \tag{3}$$

* Corresponding author.
E-mail address: diego@iafe.uba.ar (D.G. Arbó).

0168-583X/$ - see front matter © 2008 Elsevier B.V. All rights reserved.
doi:10.1016/j.nimb.2008.10.044

The value of the CEP-dependent ponderomotive energy $U_p(\varphi_{CE})$ agrees with the usual definition of the ponderomotive energy $U_p = (F_0/2\omega)^2$ only when $\varphi_{CE} = 0$. For other values of the CEP, the ponderomotive energy is reduced, i.e. $U_p(\varphi_{CE}) \leqslant U_p$. The maximum departure of $U_p(\varphi_{CE})$ from the value $U_p(0)$ occurs for sine-like pulses ($\varphi_{CE} = \pi/2$). The magnitude of the difference of the ponderomotive energy between a sine-like and a cosine-like peak ΔU_p is

$$\Delta U_p = U_p(0) - U_p(\pi/2). \quad (4)$$

Below we will analyze how the variation of $U_p(\varphi_{CE})$ affects the dominant angular momentum and the doubly differential momentum distribution near-threshold.

3. Quantum and classical electron dynamics

Angular momentum distribution have been explained by two different ionization mechanisms: (i) A biased random walk model assuming stochastic uncorrelated multiphoton processes [14] and (ii) a quasiclassical tunneling ionization process [7] calculated using classical-trajectory Monte-Carlo [15] simulations which incorporate tunneling through the potential barrier (CTMC-T). In (i), l_0 can be viewed as the most probable value after a biased random walk in momentum space assuming a stochastic uncorrelated multiphoton process: one electron with orbital quantum number l can absorb a photon and consequently undergoes a transition $l \to l+1$ with a probability p_+ or a transition $l \to l-1$ with a probability p_-, according to the dipole coupling.

In order to numerically solve the time dependent Schrödinger equation (TDSE) we employ the generalized pseudo-spectral method [16]. The calculation of the 2D momentum distribution requires projection of the wave function $|\psi(\tau/2)\rangle$ after the conclusion of the pulse onto outgoing continuum functions,

$$\frac{dP}{d\vec{k}} = \frac{1}{4\pi k}\left|\sum_l e^{i\delta_l(k)}\sqrt{2l+1}P_l(\cos\theta)\langle k,l|\psi(\tau/2)\rangle\right|^2. \quad (5)$$

Here $\delta_l(k)$ is the momentum-dependent atomic phase shift, θ is the angle between $\vec{k}$ and the polarization direction $\hat{z}$ of the laser field, P_l is the Legendre polynomial of degree l and $|k,l\rangle$ is the eigenstate of the free atomic Hamiltonian with positive eigenenergy $E = k^2/2$ and orbital quantum number l. For a rare-gas atom the atomic potential can be modeled as the sum of the asymptotic Coulomb potential plus a short-range potential that accounts for the departure from the pure coulombic behavior near the nucleus due to the screening by the other electrons [17]. In this case the atomic phase shift is the sum of the Coulomb phase shift and the phase shift due to the short-range potential [18], i.e. $\delta_l(k) = \delta_l^C(k) + \delta_l^{SR}(k)$. The latter was calculated numerically. The atom is assumed to be initially in its ground state. Due to the cylindrical symmetry for a linearly polarized laser field the magnetic quantum number remains conserved.

In Fig. 1 we show the angular distribution of the electron resulting from ionization of argon by a pulse of carrier frequency $\omega = 0.057$, peak field $F_0 = 0.065$, duration $\tau = 882$ and $\varphi_{CE} = 0$. We have projected the state at the end of the pulse onto the outgoing waves by using the atomic phase shift $\delta_l(k)$ and compare the results when only the Coulomb phase shift $\delta_l^C(k)$ is used. Some differences are observed indicating that the short-range core potential has a modest influence on the angular distribution. However, the overall structure is maintained i.e. the number of minima are the same. This is expected when the number of minima is controlled by a single angular momentum quantum number l_0, which is given directly by the partial-wave content at the end of the pulse without forming the coherent superposition (Eq. (5)).

A classical-trajectory Monte-Carlo method including tunnel effect (CTMC-T) [15,19,20] is employed to delineate the classical properties of the ionization. The CTMC-T method excludes, because

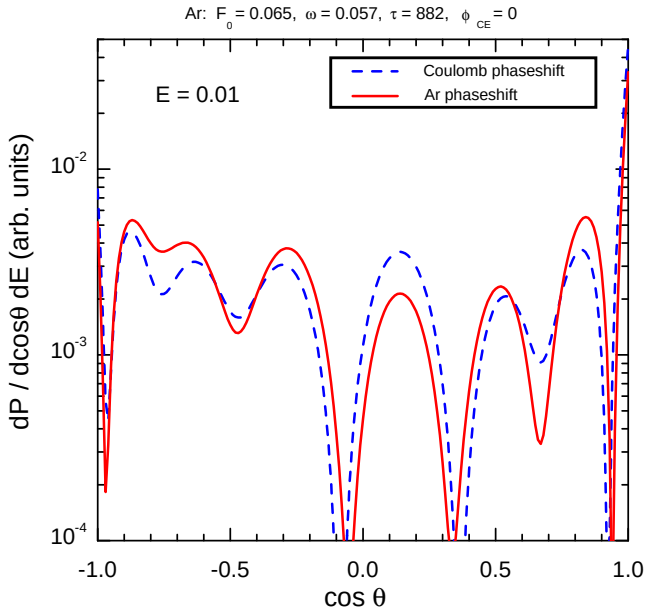

Fig. 1. Angular distribution of ejected electrons with energy $E = 0.01$ in ionization of argon by a laser of peak field $F_0 = 0.065$, frequency $\omega = 0.057$, pulse duration $\tau = 882$ and CEP $\phi_{CEP} = 0$. Dashed (blue) line corresponds to calculations performed with the Coulomb phase shift δ_l^C and solid (red) line corresponds to calculations performed with the full atomic phase shift δ_l. (For interpretation of the references in color in this figure legend, the reader is referred to the web version of this article.)

of its classical nature, any true multiphoton absorption process. The electron is allowed to tunnel through the potential barrier whenever it reaches the outer turning point, with a tunneling probability given by the WKB approximation. A typical electron trajectory after tunneling shows a quiver motion along the polarization of the laser field superimposed on a drift motion following an approximate Kepler hyperbola with the same final angular momentum [7]. As the angular momentum of the Kepler hyperbola is identical to that of the asymptotic angular momentum L of the laser-driven electron, we can identify the pericenter of the hyperbola with the quiver amplitude, $\alpha = (\sqrt{Z_T^2 + (kL)^2} - Z_T)/k^2$ with $\alpha = F_0/\omega^2$ and Z_T the asymptotic charge of the atomic potential,

$$L_0 = L(0) = (2Z_T\alpha)^{1/2}. \quad (6)$$

Two limitations should be emphasized: firstly, the classical expression does not consider dipole selection rules that may favor even or odd l_0; and secondly, L_0 is a real number while l_0 is integer. Consequently, such semiclassical estimates have an intrinsic error of $l_0 \pm 1$.

4. Results

In Fig. 2 we show the two-dimensional momentum distribution $\frac{d^2P}{dk_\rho dk_z} = 2\pi k_\rho\left(\frac{dP}{dk}\right)$ for photoionization of atomic hydrogen by a laser pulse of peak field $F_0 = 0.075$, frequency $\omega = 0.05$ and total duration $\tau = 1005$, which comprises eight cycles. In Fig. 2(a) and (b) a cosine-like ($\varphi_{CE} = 0$) and a sine-like pulse ($\varphi_{CE} = \pi/2$) are used, respectively. Both frames in Fig. 2 display complex interference patterns characterized by a transition from a ring-shaped pattern at larger k with circular nodal lines to pronounced radial nodal lines near-threshold resembling experimental results [4,5].

Differences between the photoionization due to cosine- and sine-like pulses are clearly observed near-threshold. While the first ring in Fig. 2(a) extends up to $k = 0.27$ ($E = 0.036$), in Fig. 2(b) a small ring reaches $k = 0.15$ ($E = 0.011$). In this case, the difference of the ponderomotive energy between a cosine- and sine-like pulse is, accord-

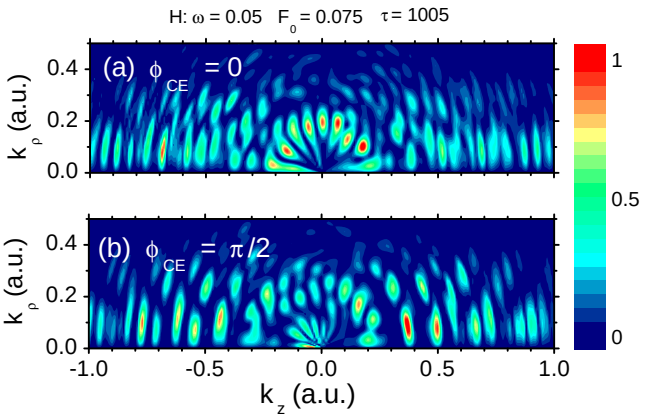

Fig. 2. Doubly differential electron momentum distributions in cylindrical coordinates (k_z, k_ρ) in photodetachment from H. The parameters of the laser field are $\omega = 0.05$, $F_0 = 0.075$, $\tau = 1005$ and (a) $\phi_{CE} = 0$ and (b) $\phi_{CE} = \pi/2$.

ing to Eq. (4), $\Delta U_p = 0.011$. The photoelectron spectrum (not shown) displays a minimum at threshold ($E = 0$) for a cosine-like pulse, which appears in Fig. 2(a) as a minimum intensity at the origin. According to conservation of energy for an N-photon process, $E = N\omega - U_p - I_p$, the spectrum should be shifted by a magnitude ΔU_p for the case of a sine-like pulse with respect to a cosine-like pulse, i.e. $E_{\sin} = E_{\cos} + \Delta U_p$. Therefore, the minimum observed at $E = 0$ for the cosine-like pulse corresponds to a shifted minimum at $E = \Delta U_p = 0.011$ ($k = 0.27$). This leads to the opening of a new channel and the appearance of a new ring of lower order in Fig. 2(b).

The two-dimensional momentum distribution of ejected electrons in ionization of argon by a laser pulse of parameters $F_0 = 0.065$, $\omega = 0.057$ and $\tau = 882$ (eight cycles) is displayed in Fig. 3. In Fig. 3(a) and (b) a cosine-like pulse and a sine-like pulse are used, respectively. According to Eq. (4), the change of the instantaneous ponderomotive energy $U_p(\varphi_{CE})$ due to the CEP-dependence is $\Delta U_p = 0.006$, about half of the one calculated for the case of Fig. 2. The photoelectron spectrum (not shown) displays no minimum at threshold as can be observed in Fig. 3(a). Therefore, a change of energy of the magnitude of ΔU_p does not imply any channel changing in the case of Fig. 3. Note that the difference between Fig. 2 and Fig. 3 stems primarily from the different field parameters and from the different ionization potential. Apart from I_p, the nature of the atomic species play a minor role [9,14].

In order to support the idea that a change in the CEP can affect the distribution of ejected electrons, we determine the distribution of contributing partial waves p_l within the first ATI ring, i.e. the partial

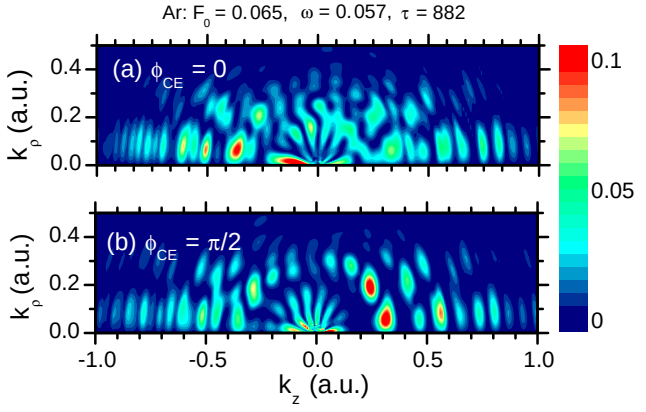

Fig. 3. Doubly differential electron momentum distributions in cylindrical coordinates (k_z, k_ρ) in photodetachment from Ar. The parameters of the laser field are $\omega = 0.057$, $F_0 = 0.065$, $\tau = 882$ and (a) $\phi_{CE} = 0$ and (b) $\phi_{CE} = \pi/2$.

ionization probability with orbital quantum number l up to the first minimum in the momentum Δ [7], $p_l = \int_0^\Delta k dk |\langle k, l|\psi(\tau)\rangle|^2$. In Fig. 2 $\Delta \simeq 0.27$ and 0.15 for the case of a cosine- and sine-like pulse, respectively, whereas in Fig. 3 $\Delta \simeq 0.25$ and 0.15 for respective cases. In Fig. 4(a) and (b) we plot the corresponding angular momentum distributions. The partial-wave distributions near-threshold peak for hydrogen and a cosine-like pulse at $l_0 = 8$ but at $l_0 = 7$ for a sine-like pulse. This decrease in one unit for the dominant angular momentum obeys the selection rule for the population of the different partial waves: as the hydrogen is initially in an s-wave ($l = 0$) and a total of $N = 22$ photons are needed to reach the continuum for the cosine-like pulse, an angular momentum distribution favoring populations of even partial waves is observed (Fig. 4(a)). In contrast, for the case of a sine pulse, $N = 21$ photons are needed to reach the continuum and, therefore, odd partial populations are favored. For the case of Fig. 3 no channel changing was observed in argon. Correspondingly, in Fig. 4(b) both calculated angular momentum distributions subject to cosine- and sine-like pulses peak at $l_0 = 7$.

Even though we have used a multiphoton picture argument above to explain a shift of the dominant angular momentum of one unit between a cosine- and a sine-like pulse, the multiphoton picture does not fully account for the near-threshold photoionization process. In Fig. 5 we show the partial-wave distributions obtained from the TDSE calculations. The partial-wave distributions near-threshold peak at $l_0 = 7$, in excellent agreement to the prediction for $L_0 = 6.8$ from Eq. (6). In order to highlight the underlying classical dynamics, we show in Fig. 5 results of the CTMC-T calcu-

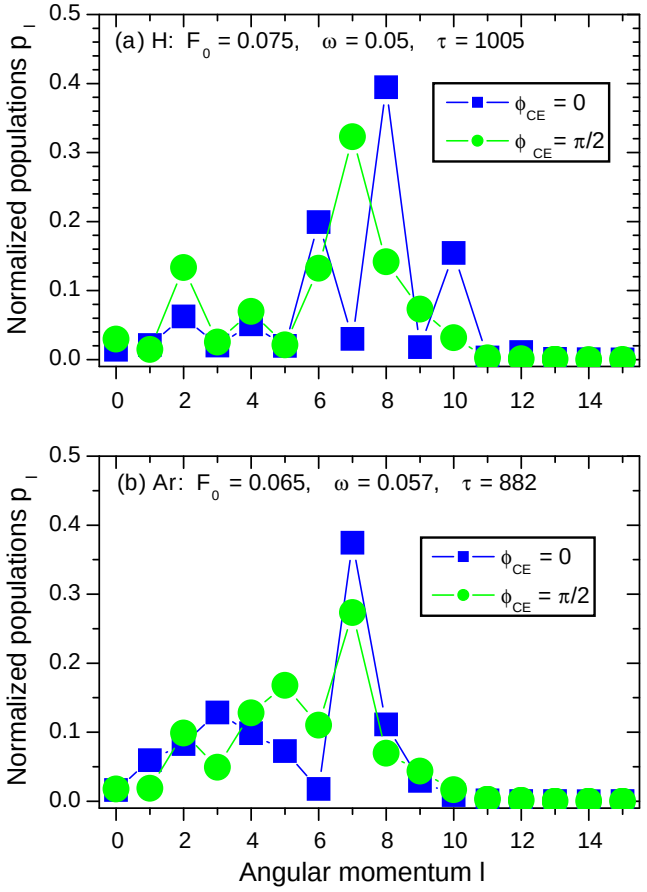

Fig. 4. TDSE partial-wave occupation probability p_l as a function of the angular momentum l for the first ATI ring (see Figs. 2 and 3) for (a) H and (b) Ar. Square dots correspond to a cosine-like pulse ($\phi_{CE} = 0$) and circular dots to a sine-like pulse (connecting lines are only meant to guide the eye). Parameters of the laser field are the same of Figs. 2 and 3 for H and Ar, respectively.

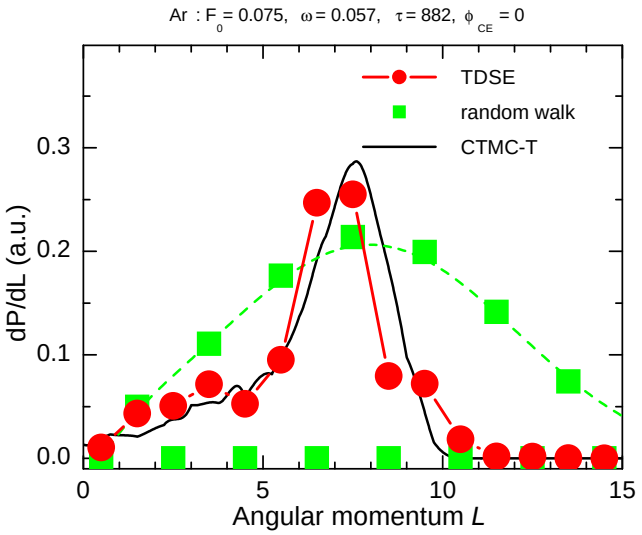

Fig. 5. Partial-wave occupation probability p_l as a function of the angular momentum l for the first ATI ring of Ar. Dots correspond to TDSE calculations and squares to the random walk multiphoton model (connecting lines are only meant to guide the eye). The solid line shows the CTMC-T quasiclassical dP/dL distribution. Parameters of the laser field are $\omega = 0.057$, $F_0 = 0.075$, $\tau = 882$ and $\phi_{CEP} = 0$. A shift $L = l + 1/2$ in the quantum calculations was added to compare to classical ones.

lations. The continuous quasiclassical angular momentum distribution dP/dL reproduces the discrete TDSE p_l distributions very well within the quantum discreteness pointing to a quasiclassical tunneling ionization picture. The width of the l-distribution can also be used to test the random walk model for the angular momentum distribution. The peak position l_0 can be well reproduced by choosing $p_+ = 2/3$ and $p_- = 1/3$ (see Section 3) in a Poissonian random walk process. However, the peak position l_0 and the width σ of the angular momentum distribution are interrelated and both are proportional to N. Consequently, we find a broad p_l distribution in Fig. 5 at variance with both the TDSE and the quasiclassical CTMC-T results. The latter clearly shows the sub-Poissonian nature of the interaction process proper of the tunneling regime for Keldysh parameters near unity.

5. Conclusion

For photoionization of atoms by few-cycle laser pulses we have shown that the dependence of the instantaneous ponderomotive energy at the peak field on the CEP can induce channel closings and lead to changes in the photoelectron momentum distribution. Hence, the dominant angular momenta near-threshold can also depend on the CEP and this should be added to the quantum uncertainties explained in [9]. Despite this multiphoton characteristics stemming from the selection rule for the angular momentum, the narrow angular momentum distribution near-threshold is the result of a tunneling process at variance with a broad Poissonian distribution resulting from a biased random walk model.

Acknowledgements

D.G.A. thanks Jorge Miraglia for discussions about the full atomic phase shift. This work was performed with financial support of CONICET and ANPCYT (PICT 772) of Argentina, by the SFB 016 ADLIS and the Project P15025-N08 of the FWF (Austria) and by the EU Projects HPRI-2001-50036 and HPRI-CT-2005-026015.

References

[1] G.G. Paulus, F. Grasbon, H. Walther, P. Villoresi, M. Nisoli, S. Stagira, E. Priori, S. De Silvestri, Nature (London) 414 (2001) 182;
A. Apolonski et al., Phys. Rev. Lett. 92 (2004) 073902.
[2] C.P.J. Martiny, L.B. Madsen, Phys. Rev. Lett. 97 (2006) 093001.
[3] F. Lindner, M.G. Schätzel, H. Walther, A. Baltuška, E. Goulielmakis, F. Krausz, D.B. Milošević, D. Bauer, W. Becker, G.G. Paulus, Phys. Rev. Lett. 95 (2005) 040401.
[4] A. Rudenko, K. Zrost, C.D. Schröter, V.L.B. de Jesus, B. Feuerstein, R. Moshammer, J. Ullrich, J. Phys. B 37 (2004) L407.
[5] C.M. Maharjan, A.S. Alnaser, I. Litvinyuk, P. Ranitovic, C.L. Cocke, J. Phys. B 39 (2006) 1955.
[6] A. de Bohan, Ph.D. Thesis, Université Catholique de Louvain, 2001.
[7] D.G. Arbó, S. Yoshida, E. Persson, K.I. Dimitriou, J. Burgdörfer, Phys. Rev. Lett. 96 (2006) 143003.
[8] D.G. Arbó, J.E. Miraglia, M.S. Gravielle, K. Schiessl, E. Persson, J. Burgdörfer, Phys. Rev. A 77 (2008) 013401.
[9] D.G. Arbó, K.I. Dimitriou, E. Persson, J. Burgdörfer, Phys. Rev. A 78 (2008) 013406.
[10] M. Wickenhauser, X-M. Tong, C.D. Lin, Phys. Rev. A 73 (2006) 011401.
[11] G.G. Paulus, F. Grasbon, H. Walther, R. Kopold, W. Becker, Phys. Rev. A 64 (2001) 021401.
[12] R. Kopold, W. Becker, M. Kleber, G.G. Paulus, J. Phys. B 35 (2002) 217.
[13] D.B. Milošević, E. Hasović, M. Busuladži ć, A. Gazibegović-Busuladžić, W. Becker, Phys. Rev. A 76 (2007) 053410.
[14] Z. Chen, T. Morishita, A-T. Le, M. Wickenhauser, X.M. Tong, C.D. Lin, Phys. Rev. A 74 (2006) 053405.
[15] K.I. Dimitriou, D.G. Arbó, S. Yoshida, E. Persson, J. Burgdörfer, Phys. Rev. A 70 (2004) 061401(R).
[16] X.-M. Tong, S.I. Chu, Chem. Phys. 217 (1997) 119.
[17] H.G. Muller, F.C. Kooiman, Phys. Rev. Lett. 81 (1998) 1207.
[18] H. Friedrich, Theoretical Atomic Physics, Springer-Verlag, Berlin, 2006.
[19] J.S. Cohen, Phys. Rev. A 64 (2001) 043412;
J.S. Cohen, Phys. Rev. A 68 (2003) 033409.
[20] S. Borbély, K. Tőkési, L. Nagy, Phys. Rev. A 77 (2008) 033412.